Science of the Total Environment 824 (2022) 153790

Contents lists available at ScienceDirect

Science of the Total Environment

journal homepage: www.elsevier.com/locate/scitotenv

Piezo-photocatalytic flexible PAN/TiO_2 composite nanofibers for environmental remediation

Deng Ding [a], Zhiwei Li [b], Sooyung Yu [c], Bingxin Yang [c], Yadong Yin [b], Ling Zan [d], Nosang Vincent Myung [c,*]

[a] College of Chemistry and Environmental Engineering, Wuhan Polytechnic University, Wuhan 430023, China
[b] Department of Chemistry, University of California, Riverside, California 92521, USA
[c] Department of Chemical and Biomolecular Engineering, University of Notre Dame, IN 46556, USA
[d] College of Chemistry and Molecular Science, Wuhan University, Wuhan 430072, China

HIGHLIGHTS

- The photocatalytic activity of PAN/TiO_2 nanofiber mat can be promoted by harvesting environmental mechanical energy.
- Enhancing the catalytic activity of mat were attributed to piezoelectric output voltages.
- The piezoelectric output voltages depend on the diameter of nanofiber and content of PAN and TiO_2.
- The mechanism for enhanced photocatalytic activity of nanofiber composite is proposed.

GRAPHICAL ABSTRACT

Flexible TiO_2/PAN composite nanofibers as piezo-photocatalyst.

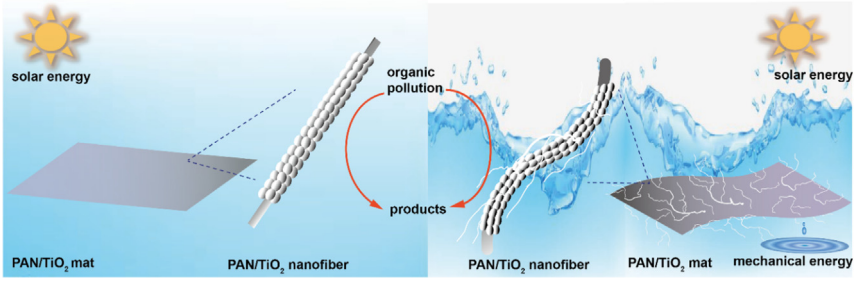

ARTICLE INFO

Article history:
Received 9 December 2021
Received in revised form 5 February 2022
Accepted 6 February 2022
Available online 9 February 2022

Editor: Jay Gan

Keywords:
Photocatalysis
Piezocatalysis
Piezoelectricity
Polyacrylonitrile
Titanium dioxide
Electrospinning
Nanofiber

ABSTRACT

Mechanical vibrations and solar energy are ubiquitous in the environment. Hereon, we report the synergic enhancement of the oxidation by simultaneously harvesting solar and mechanical vibrations through flexible piezo and photocatalytic composite nanofiber mats. Surface enriched titanium dioxide nanoparticles incorporated in polyacrylonitrile (PAN/TiO_2) nanofibers were synthesized using a single pot electrospinning process with well-defined fiber diameters with widely tunable loading density. By incorporating photocatalytic TiO_2 in flexible piezoelectric PAN nanofiber support, piezoelectric fields generated under the mechanical deformation promote the separation of the photogenerated electrons and holes to accelerate oxidation of pollutants. Our results demonstrated that the catalytic activity of PAN/TiO_2 nanofibers in photodegradation of Rhodamine B (RhB) can be greatly enhanced by environmental vibration-induced piezoelectricity of PAN nanofibers, with a maximum enhancement factor of ~2.5. The working mechanism for the enhanced photocatalytic activity of PAN/TiO_2 nanofibers by the mechanical vibrations were attributed to the piezoelectric effect of PAN nanofibers, which could efficiently promote the separation of the photogenerated electrons and holes in the TiO_2 nanoparticles. We believe the approach to enhancing the catalytic activity of mat can make full use of the polymer properties and natural energy, and it also can be extended to other composite polymer/semiconductor systems.

1. Introduction

Energy efficient wastewater treatment is one of highest priority to reduce costs and improve environmental sustainability. To achieve this goal, solar driven photocatalytic oxidation has been extensively studies for degradation of contaminants (Hisatomi et al., 2014; Ong et al., 2016; Brillas and Martínez-Huitle, 2015). Pure and doped TiO_2 nanostructures

* Corresponding author at: McCourtney Hall 105D Notre Dame, Notre Dame, IN 46556, USA.
E-mail address: nmyung@nd.edu (N.V. Myung).

http://dx.doi.org/10.1016/j.scitotenv.2022.153790

mostly widely used photo catalysts due to their high stability, low-cost, and eco-friendliness (Zhou et al., 2016; Crossland et al., 2013; Zeng et al., 2019; Ou et al., 2016; Nalbandian et al., 2015a; Nalbandian et al., 2015b; Shuai et al., 2013; Nalbandian et al., 2012). However, these nanostructures easily aggregate in environment owing to their high surface energy which lower photocatalytic activities. Additionally, they are difficult to separate and recycle from the treated solution which also limits long-term use (Wang et al., 2016; Chou et al., 2013; Senthamizhan et al., 2016; Zhou et al., 2018; Wang et al., 2018). To overcome these obstacles, a few research groups including our group reported nanoparticles decorated polymeric nanofiber mats where polymeric nanofiber serve as solid support for easier separation after treatment (Zhou et al., 2018; Xi et al., 2014; Greenstein et al., 2019; Peter et al., 2016).

Low-quality mechanical vibrations are also ubiquitous in the environment. Recently, piezocatalysis has been demonstrated to remediate pollutants by harvesting mechanical vibration into electrical energy through piezoelectric materials (Chorsi et al., 2019). It is a well-known effect that involves the production of an electric potential in piezoelectric materials with non-centrosymmetric structures (Tu et al., 2020). The electric potential as static electric fields have an effect on separation and migration of carriers (Chen et al., 2019). Wang et al. reported that ZnO nanorods with non-centrosymmetric structures can produce electricity by applying mechanical stress. The piezo-induced bias voltage promotes the separation of electrons and holes, leading to the enhanced quantum efficiency of these static internal electric fields (Liang et al., 2019). Other perovskite-type piezocatalysts such as $BiFeO_3$ $NaNbO_3$, $PbTiO_3$, $ZnSnO_3$ and CdS have also been investigated to some extent (Tu et al., 2020; Mushtaq et al., 2018; Amiri et al., 2020; Zhao et al., 2019). Except for that, the electric fields of piezoelectric materials were reported to enhance the non-piezoelectric materials (*e.g.*, TiO_2, Ag_3PO_4). Chi Lo et al. combine both the piezo-property of $BaTiO_3$ and the photo-property of Ag_3PO_4 and promote the separation of the photo-generated electron–hole pairs of Ag_3PO_4 (Lan et al., 2019). However, most reports prove the piezoelectic effect on the photocatalytic activity by studying on nanoparticles. The piezoelectric materials usually produce piezoelectric by the ultrasonic wave, while the ultrasonic bring a better dispersion of nanoparticles. Actually, the dispersion has much effect on the photocatalytic activity, a better dispersion of nanoparticles will avoid aggregation to obtain bigger catalytic surface area. Therefore, the enhanced photocatalytic activity maybe come from the dispersion instead of piezoelectric effect. To prove the piezoelectric effect on the photocatalysis completely, the electrospinning method are provided to synthesize nanofiber/catalyst composite membranes, nanoparticles will be fixed on the fiber to prevent dispersion. What's more, the composite membranes are promising in high-performance water remediation largely because they have high surface areas, high length–diameter ratios, good flexibility, and low cost (Zhou et al., 2018; Xi et al., 2014).

Electrospun polyacrylonitrile (PAN) nanofibers are long one-dimensional (1D) nanostructures with good chemical stability and excellent flexibility (Yu and Myung, 2018). Additionally, they show significantly enhanced piezoelectric properties compared to thin film counterparts due the preferential crystal formation of electroactive phases during the process (Wang et al., 2019). Further, it is easier to create greater strain with given stress due to their geometry and flexibility (Chorsi et al., 2019; Nonnenmann et al., 2010). To take these advantages, here, we combine the photocatalytic properties of TiO_2 nanoparticles with piezocatalytic properties of PAN nanofibers for enhanced catalytic degradation of pollutants by simultaneously harvesting solar and mechanical energies (Fig. 1). PAN/TiO_2 composite nanofiber mat with a different diameter and loading density were fabricated by electrospinning. The content and size dependent piezoelectric properties of nanofibers were systematically investigated first followed by catalytic decomposition of Rhodamine B under vibration, solar illumination and their combination. A governing mechanism was also proposed through independent analysis of the charge separation experiment.

2. Experimental section

2.1. Experimental materials

Titanium dioxide nanoparticles (Aeroxide® P25), Polyacrylonitrile (PAN; MW = 150,000) and *N*, *N*-dimethylformamide (DMF) was purchased from Thermo-Fisher Scientific. The surfactant cetyltrimethylammonium bromide (CTAB; ≥98%) was obtained from Aldrich. All chemicals were used without further treatment.

2.2. Experimental methods

2.2.1. Electrospinning sol-gel solutions to control diameter

Composite nanofiber with different diameter were prepared by varying PAN wt% in the solution while fixing mass ratio of PAN and TiO_2 (1 to 2) in 10 ml DMF. CTAB concentration was fixed for all solutions. Once all components are homogeneously mixed by magnetic stirring, the solution was also treated by sonication for at least 1 h. At last, the solution was stirred again at room temperature for at least 6 h. The samples with 4 wt%, 5.5 wt%, 7 wt % PAN were named as 4%PAN/2TiO_2, 5.5%PAN/2TiO_2 and 7%PAN/2TiO_2, respectively.

2.2.2. Electrospinning sol-gel solutions to control TiO_2 loading density

Composite nanofibers with different TiO_2 loading density were prepared by varying TiO_2 wt% in the solution while fixing PAN and CTAB at 4 and 1 wt%, respectively, in 10 ml DMF. The solution was treated the same way as above. The samples with different weight percentage of TiO_2 ranges from 2 wt% to 16 wt% were named as 2%PAN/TiO_2, 4%PAN/TiO_2, 6%PAN/TiO_2, 8%PAN/TiO_2, 10%PAN/TiO_2, 12%PAN/TiO_2 and 16%PAN/TiO_2. (The detailed data was shown in Table S1).

2.2.3. Electrospinning conditions

Electrospinning conditions followed the previously reported work (Yu and Myung, 2018). Briefly, the solutions were placed in a 5-mL BD Luer-Lok syringe and electrospun for 6 h at an applied voltage of 15 kV between needle and drum collector (Fig. S1). The electrospinning environmental

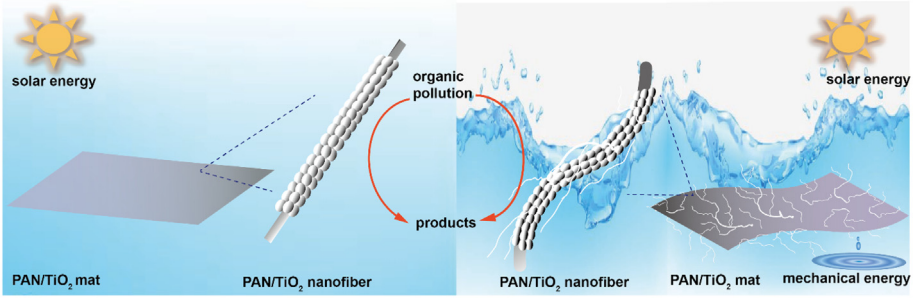

Fig. 1. Schematic representation of the photocatalytic degradation RhB using TiO_2/PAN membrane under simultaneously exposure to solar illumination and mechanical vibration.

condition was set to be 25 °C and 60% respectively. The collector rotation speed was fixed at 400 rpm (Dingtuo Technology).

2.3. Material characterization

X-ray diffraction (XRD) patterns of the samples were determined using PANalytical Empyrean Series 2 X-ray diffractometer using Cu Ka radiation at a scan rate of 4° min^{-1} over 2θ ranging from 10 to 70°. The morphologies of PAN/TiO_2 composite nanofibers were characterized using a VEGA3 scanning electron microscope (SEM) (Tescan Brno, Czech Republic). Fiber diameter was assessed using Image J software. Brunaer–Emmett–Teller (BET) studies were done to calculate surface area and Barret–Joyner–Halenda (BJH) analysis were done for pore size distribution studies using same N2 adsorption–desorption isotherm (Autosorb iQ station 2).

2.4. Piezoelectric characterization

The collected PAN/TiO_2 nanofiber mat were cut into 1 cm × 4 cm. The sample was fixed between two copper plates coated by a strip of polyimide tape (Fig. S2). The bending and releasing motion were controlled by a custom-made vibrational system. The prepared samples were fixed on a cantilever holder. Then the system was mounted on the top of the diaphragm of a subwoofer speaker. A GoPro Hero3 + camera (GoPro, Inc., San Mateo, CA) was also fixed aside to record the bending motion. The generated voltage was measured by an oscilloscope (Pico Technology, St Neots), when the subwoofer speaker sounds 10 Hz.

2.5. Photoelectrochemical measurements

Photo-electrochemical measurements were carried out in a three-electrode quartz cell with the CHI-760C electrochemical system. Ag/AgCl (3 M KCl) electrode was used as the reference electrode, and platinum wire served as the counter electrode. To prepare the working electrode, the 1 cm × 1 cm nanofiber mat was fixed onto an indium tin oxide (ITO) coated glass slide by a tape with a round blank tape in the middle. A conducted copper tape contacted the mat to conduct electricity. Then the ITO glass was fixed on a microscope slide after the glass was sealed with a strip of polyimide tape except for the round blank. Fig. S3 shows the assembled work electrode. Aqueous sodium sulfate (*i.e.,* 0.5 M Na_2SO_4) was used as the electrolyte with a 350 W Xenon lamp as the solar simulator. An ultrasonic unit was applied to cause water vibration. The current as a function of time was measured at a fixed applied potential of + 0.5 V *vs.* Ag/AgCl by using the electrochemical workstation under vibration, solar illumination and their combination.

2.6. Electron paramagnetic resonance (EPR) experiments

Electron paramagnetic resonance (EPR) signals of produced OH- and O2− were recorded by an EPR spectrometer (EPR200M; CIQTEK, China) with a modulation of 100 kHz and a microwave frequency of 9.77 GHz. The 5,5-dimethyl-1-pyrroline-N-oxide (DMPO) was used as spin-trapping reagents. For the detail spin trapping of OH-, 10 mg TiO_2/PAN mat were premixed with 1 mL water and 5ul DMPO. After being treated by vibration, illuminate or vibrate-illuminate for 40 s separately, the solution was characterized into the EPR testing quartz tube at room temperature. For the spin trapping of O2−,10 mg TiO_2/PAN mat were premixed with 1 mL methanol and 20ul DMPO. The mixed sample were treated for 20s under vibration, illuminate or vibrate-illuminate.

2.7. Catalytic activity measurement

50 mg of circular PAN/TiO_2 nanofiber met was cut and placed in a round bracket. The bracket was fixed in a container wrapped in aluminum foil. Then 100 mL of RhB solution (5 mg/L) was added in it. Before illumination or vibration, the suspension was in the dark for at least 2.0 h at room temperature to make sure that the adsorption-desorption equilibrium was achieved. During illumination or vibration, 1.0 mL suspension was sampled from the reactor at every 10 min. The clear liquid was analyzed by recording the maximum absorption band (553 nm for RhB) using an Ocean Optics Flame-S-XR1-ES spectrophotometer.

3. Result and discussion

PAN/TiO_2 composite nanofiber membrane were flexible and tailorable by various electrospinning precursor solution (Fig. S1). As shown in Fig. 2, electrospun PAN/TiO_2 nanofiber mats were uniform in diameters where most of the TiO_2 nanoparticles were exposed on their surface. By tuning the electrospinning solution (*e.g.,* PAN content), the diameter of composite nanofibers was readily tuned (Figs. 2a–c and S5) while maintaining the composition of composite nanofibers. Figs. 2e–g and S6 show the morphology of nanofibers with different TiO_2 contents where the average diameter also increased with TiO_2 content with a fixed PAN content (Fig. 2g).

The XRD was used to confirm the presence of TiO_2 nanoparticles and their crystals structures in the composite nanofiber mat. The TiO_2 utilized

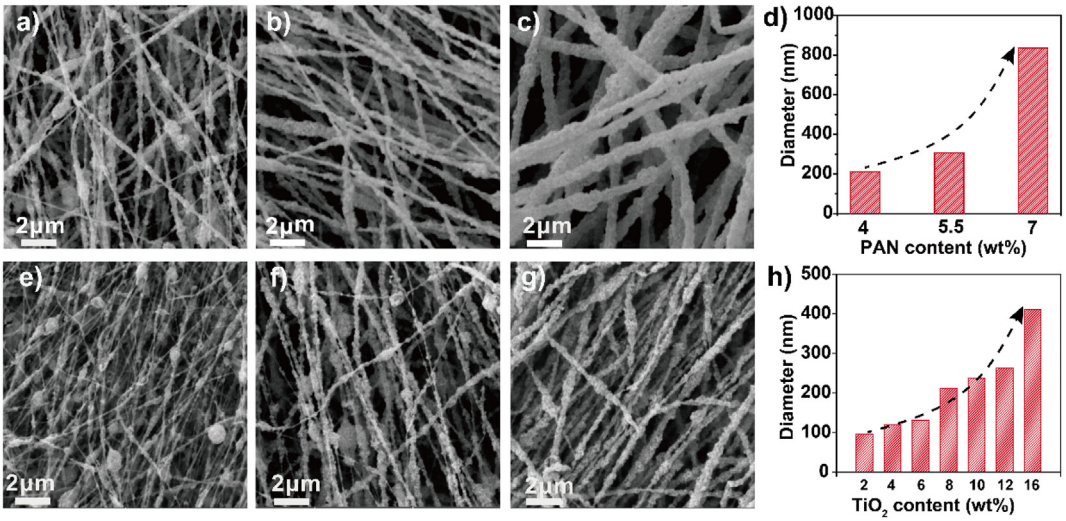

Fig. 2. SEM images of electrospun PAN/TiO_2 nanofibers with different diameter by varying PAN wt% while fixing PAN/2TiO_2 ratio at 0.5 (a–c) and PAN/TiO_2 nanofibers with various PAN/TiO_2 ratio (*i.e.*, 1 to 4) while fixing PAN content at 4 wt% (e–g). The average diameters of PAN/TiO_2 nanofibers as function of PAN (d) and TiO_2 (h) contents.

in this work is a commercial TiO_2 nanoparticle consisted of 80% anatase and 20% rutile phases (Ding et al., 2020). In Fig. S4, The XRD pattern of Pure TiO_2 and PAN/TiO_2 composite films were in agreement with the standard card, (PDF#21–1272 and PDF#21–1276) (Yu et al., 2017), which confirms the presence of TiO_2 and their remained crystal structureTiO_2.

To gain insight into the surface area of the nanofibers, the BET analysis was done using N2 adsorption–desorption method. In the Fig. S13, it represents N_2 adsorption–desorption isotherms of PAN nanofiber, 4%PAN/TiO_2, 8%PAN/TiO_2, 16%PAN/TiO_2. The specific surface area of PAN nanofiber was 25.0 m^2/g while 4%PAN/TiO_2, 8%PAN/TiO_2, 16%PAN/TiO_2 were found to be 19.5 m^2/g, 16.7 m^2/g and 9.3 m^2/g, respectively (Table S5). The Fig. S14 revealed that the specific surface area deceased with the TiO_2 content increasing. It can be attributed to the increasing diameter of nanofiber with the TiO_2 content increasing.

To confirm the piezoelectric performance of PAN/TiO_2 composite nanofiber mats under strains, the nanofiber mats were subjected to a mechanical bending and releasing motion and the two opposite pulse output voltages were showed in the Fig. S7. The repeated bending-releasing motion resulted in multiple signals of output voltages in the Fig. 3a and b. It can be concluded that all PAN/TiO_2 composites remain the piezoelectric property (Wang et al., 2019; Ico et al., 2018). To further investigate effect on piezoelectric performances of PAN/2TiO_2 with different PAN contents, the output voltages were measured under different bending strain as showed in the Fig. S7. The output voltage was increasing with strain increasing (Chorsi et al., 2019). Fig. 3a shows the output voltage signals of PAN/2TiO_2 nanofibers with different PAN contents under bending strain of about 1.0%. The 4%PAN/2TiO_2 had a maximum output voltage of 520 mV, while the 5% PAN/2TiO_2 and 7% PAN/2TiO_2 nanofiber mats had 100 mV and 80 mV respectively. Obviously, the output voltages were decreasing with PAN increasing. This can be caused by the different diameters of PAN/2TiO_2 composites. In the Fig. S9a, it revealed that the bigger diameter can bring to a smaller output voltage. The result was the same as that of PVDF reported previously (Ico et al., 2018). Also, the effect of TiO_2 contents on the PAN/TiO_2 were investigated and discussed. The results exhibited the same relationship between output voltage and strain as above conclusion (Fig. S8). The Fig. 3c presents the output voltage signals of PAN/TiO_2 nanofibers with increasing the TiO_2 content from 0 wt% to 16 wt% under bending strain of about 1.0%. The output voltages were increasing with the increasing TiO_2 content in the composite. This can be explained by that the TiO_2 does not show a piezoelectric property.

Based on these results, all PAN/TiO_2 composite nanofiber mat show piezoelectricity. Hence, to investigate the effect of piezoelectricity of PAN/TiO_2 nanofiber mat on the photocatalytic activity, the photo-degradation of organic molecular RhB was used to evaluate the photocatalytic activities of as-prepared samples under vibration, UV light and their combination. In the Figs. 4 (a), (d) and S10, the RhB can be degradated under vibration, solar and vibration-solar. To analyze the effect of vibration and PAN content on catalytic activity, the reaction kinetics were treated as pseudo-first-order and it was written as follow Eq. (1) (Gao et al., 2016):

$$\ln (C_0/C) = kt \quad (1)$$

The rate constant k can be calculated by the linear fitting of the plot of ln (C_0/C) *versus* t (Fig. S10) (Ma et al., 2019). Fig. 4b exhibits the comparison of rate constant k for as-prepared PAN/2TiO_2 nanofiber mats with different PAN contents. Obviously, all samples showed better photocatalytic activity under vibration-solar than that under only vibration or solar light. It revealed that the vibration of PAN/2TiO_2 nanofiber mats can enhance the catalytic activity. In addition, the rate constant k decreased as the PAN contents increased from 4% to 7%, which suggested a lower PAN content leaded to a higher enhancement on the photocatalytic activity. This may be attributed to lower PAN content and smaller diameter of 4%PAN/2TiO_2 nanofibers than that of 5.5%PAN/2TiO_2 and 7%PAN/2TiO_2

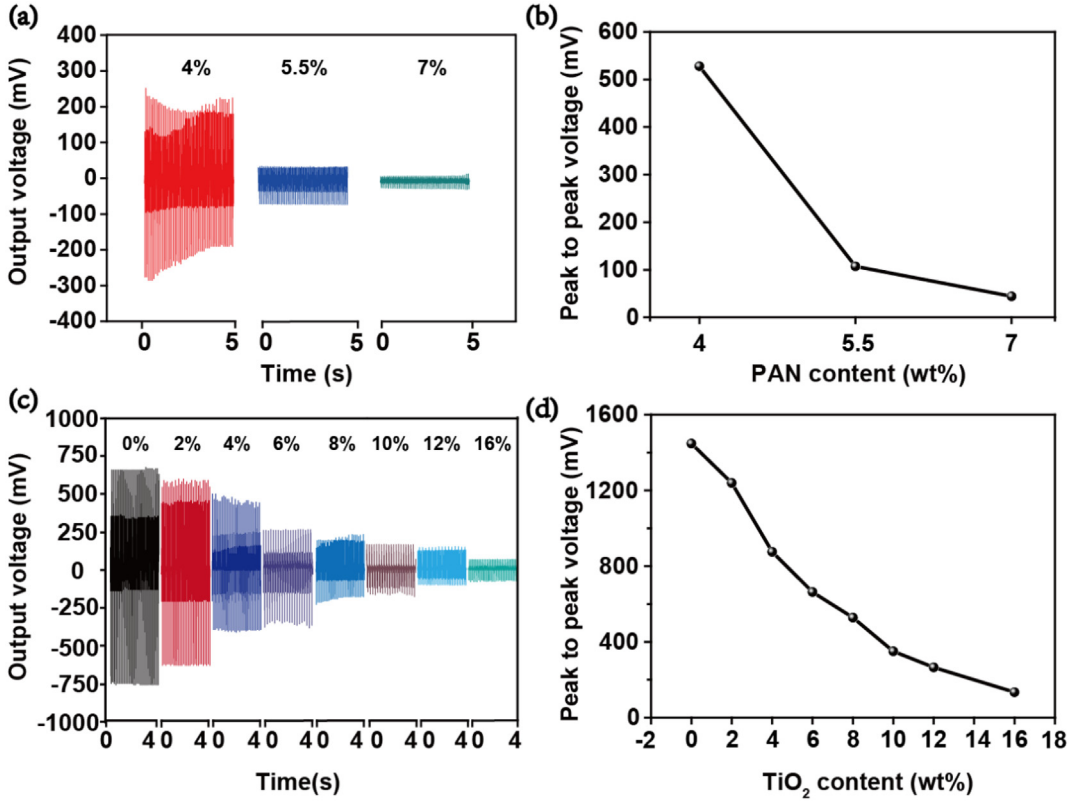

Fig. 3. (a) Output voltages of PAN/2TiO_2 nanofibers prepared by using different PAN contents under mechanical bending/releasing and (b) their peak-to-peak voltages. The ratio between PAN and TiO_2 remains 1 to 2. (c) Output voltages of PAN/TiO_2 nanofibers prepared by increasing the TiO_2 content from 0 wt% to 16 wt% under mechanical bending/releasing and (d) their peak-to-peak voltages.

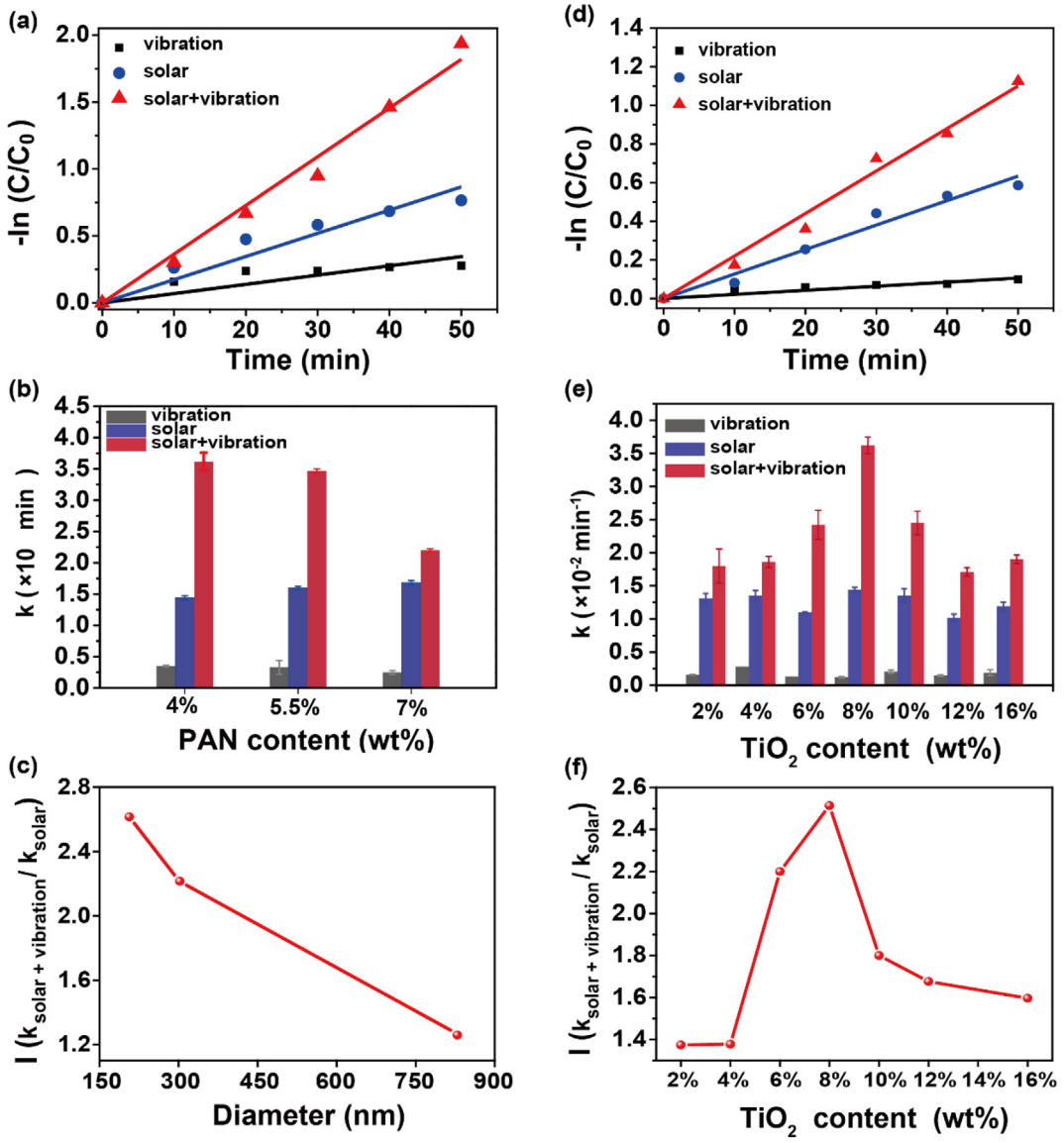

Fig. 4. Catalytic degradation RhB rate(k) of pseudo-first-order reaction under light, vibration, and their combination for (a) PAN/2TiO_2 nanofibers with different PAN content and (d) PAN/TiO_2 with different TiO_2 content; Comparison of rate (k) of PAN/$TiO_2$with (b) different PAN contents (e)different TiO_2. (c) The enhancement factor for PAN/2TiO_2 nanofibers with different diameter; the enhancement factor for PAN/TiO_2 nanofibers with the TiO_2content increasing from 2 wt% to 16 wt%.

nanofibers. In Fig. 4c, the enhancement factor I ($k_{solar + ultrasonic}/k_{solar}$) decreased with the dimeter increasing. Based on above results of relation between dimeter and piezoelectric output voltage, it can be concluded that higher piezoelectric output voltage leads to a larger enhancement factor when the ratio of PAN and TiO_2 remain a fixed value of 1 to 2.

The effects of TiO_2 contents were also discussed with a fixed PAN content and different TiO_2 contents by the same valuate method. Similarly, the RhB can be degraded by the as-prepared PAN/TiO_2 nanofiber mats under vibration, solar and vibration-solar. Fig. S11 and Fig. 4e exhibits all rate constant k values of PAN/TiO_2 nanofiber mats with TiO_2 loading content increasing from 2% to 16%. It was obvious that the photocatalytic activities of all PAN/TiO_2 nanofiber mats were enhanced under the solar-vibration which is consistent with the above results. In the Fig. 4f, it was observed that the enhancement factors I increased with the increased content of TiO_2 from 2 wt% to 8 wt%, while it decreased with the further increases of TiO_2 contents from 8 wt% to 16 wt%. The optimal content of TiO_2 was 8 wt% for the highest photocatalytic activity for degradation of RhB. During the catalytic degradation, the photocatalytic activities of the nanofiber mat increased with the TiO_2 content increasing from 2% to 8%. However, with the TiO_2 content increasing continuously, the piezoelectricity voltage was decreasing gradually so that the effect of piezoelectricity on TiO_2 were deceasing. Also, the optimal piezo-photocatalytic activities of PAN/TiO_2 nanofiber mats were compared with the results with other systems in the Table S4.

In photocatalytic wastewater treatment systems, the adsorption effection and pH of solution have an effect on the rate of degradation (Huang et al., 2008). Herin, the effects were investigated.

In the Fig. 5 and Table S1, the adsorption effection of composite membrane for RhB were observed. It showed the adsorption percentage of PAN/TiO_2 nanofibers with different contents, when it achieved to absorbance of adsorption equilibrium. All composite PAN/TiO_2 have an adsorption effection for RhB, the adsorption percentage exhibtes a little bit slowdown with TiO_2 content from 0 wt% to 16 wt%. In the Fig. 5, it was observed that the piezo-photocatalytic degradation RhB rate (k) increased with the content of TiO_2 from 2 wt% to 8 wt%, while it decreased with the further increases of TiO_2 contents. Comparing the two change behaviors, it indicated the adsorption effects is not the main factors on piezo-photocatalysis of PAN/TiO_2 nanofibers.

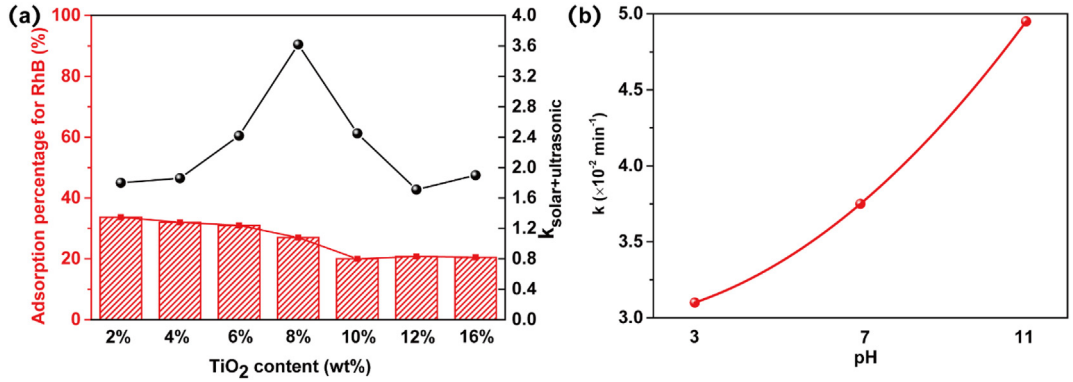

Fig. 5. (a) RhB adsorption percentage and piezo-photocatalytic degradation RhB rate(k) of PAN/TiO_2 nanofibers prepared by increasing the TiO_2 content from 0 wt% to 16 wt%; (b) The effect of pH values of RhB on piezo-photocatalytic degradation by PAN/TiO_2 (4 wt% PAN and 8 wt% TiO_2).

pH value is also a factor influencing the rate of degradation. In Fig. 5, it clearly suggested that the piezo-photocatalytic rate is also increasing with pH value increasing. It attributes to ionization reactions of TiO_2 surface under different pH value. The ionization reactions are as follows:

$$TiOH + H^+ \rightarrow TiOH^+_2$$

$$TiOH + OH^- \rightarrow TiO^- + H_2O$$

According to the reactions, the pH value can change the surface charge status of TiO_2. The status has an effect on the adsorption of dye molecules onto the TiO_2 surfaces, while the adsorption of dye is important for catalytic reactions.

When the solution was acid, the surface of TiO_2 exhibited positive charge. It became difficult to adsorb the RhB with cationic form due to an electrostatic repulsive force and it will slow down the rate of degradation (You-ji and Wei, 2011). Conversely, when the solution was alkaline, it would take a better adsorption of RhB, thus the rate piezo-photocatalytic of degradation is enhanced.

To investigate the stability of PAN/TiO_2, the five circulating experiments runs in the degradation of RhB under Uv-light and vibration. As shown in Fig. S12, PAN/TiO_2 still has effective degradation with a slight activity after five cycles, indicating the excellent stability of PAN/TiO_2 in the application of RhB degradation.

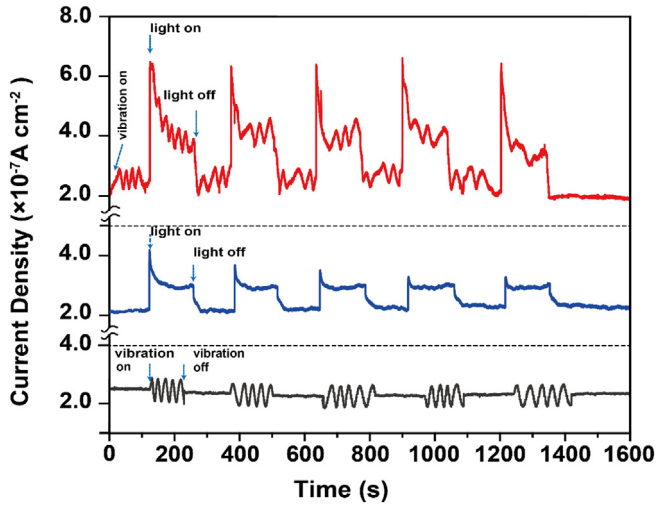

Fig. 6. Transient current responses of the PAN/TiO_2 nanofibers measured in 0.5 M Na_2SO_4 aqueous solution by using 4 wt% PAN and 8 wt% TiO_2 under different conditions.

Admittedly, based on the results, it proves that the piezoelectricity of PAN nanofibers can enhance the photocatalytic activity of TiO_2. To clarify the reason, the transient photocurrent (TPC) measurement are used to investigate the separation of efficiency of photogenerated carries occurring on the composite catalyst, which is very important for the efficiency of photocatalytic reaction (Raziq et al., 2018). In the Fig. 6, the signals of TPC were detected by controlling the on-off cycles under vibration, UV light and their combination. When there was only vibration, the 4%PAN/TiO_2 nanofiber showed the multiple undulate signals of PAN piezoelectric current, which was same as the results in Fig. 2. The photocurrent increased positively under the light illumination, which was caused by TiO_2 as reported in previous literature (Shi et al., 2020). Under vibration and illumination, the signals of current consist of above piezoelectric current and photocurrent, which is same phenomenon with that reported by Yue (Chen et al., 2017; Lin et al., 2014). It is obvious that the photocurrent in the compound current exhibited stronger than that under illumination. Therefore, it suggests that the separation of efficiency of photogenerated carries of TiO_2 in the PAN/TiO_2 nanofiber composite was improved owing to the piezoelectricity of PAN.

The reactive radicals produced from 8%PAN/TiO2 were investigated by electron spin resonance (ESR). The Fig. 7 showed ·OH and O_2^- radicals produced under vibration, UV light and their combination, it indicated the holes and electrons can drive the formation of ·OH and O2- radicals. In Fig. 7a, there is no characteristic peak of DMPO·OH under vibration, while the obvious quadruple peak of DMPO-·OH could be observed under illumination (Chen et al., 2021; 1-s2.0-S138589472102739X-main.pdf, n.d.). When the PAN/TiO_2 nanofiber mats were under vibration and illumination, the signal of DMPO-•OH is slightly greater than that observed under illumination. The result indicated that ·OH radicals are mainly generated by the illumination, while much more ·OH radicals can produce under vibration and illumination. Distinctly, the DMPO-•O2− signals produced under illumination and vibration are much stronger than that observed under illumination in the Fig. 7b. When there was only vibration, there was hard to detect the DMPO-•O2− signals. it suggests that the •O2− radicals are mainly generated by the illumination excitation, while the vibration can promote •OH radicals under illumination. Also, the change rules of two radicals produced under different condition are consistent with that of Catalytic degradation RhB shown in the Fig. 4. Therefore, it indicted that PAN/TiO_2 nanofiber mats can boost the generation of •OH and O_2^- radicals under solar and vibration, thereby promoting the photocatalytic activity of PAN/TiO_2 for degradation RhB.

In the Fig. 8, a mechanism was proposed according to the above results. When the PAN/TiO_2 nanofibers was illuminated, the photo-generated carriers will be excited and migrate to the surface randomly show in the Fig. 8. It is easy to happen for combination of photo-generated electrons and holes (Chen et al., 2021). Therefore, there is only a little photo-generated electrons and holes used to photocatalytic reaction, it limits the efficiency of

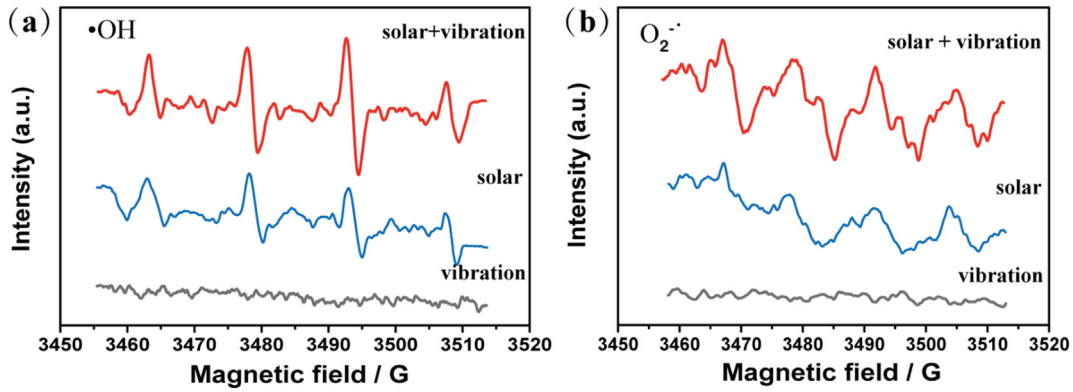

Fig. 7. DMPO spin-trapping ESR spectra of 4 wt% PAN and 8 wt% TiO_2 under vibration, UV light and their combination for (a) DMPO-·OH radical; (b) DMPO-$·O_2$- radical.

catalytic degradation. While the nanofibers were bended under the vibration caused by water wave, the surface of PAN nanofibers will exhibit the positive and negative charges owing to polarization (Wang et al., 2019; Ueda and Carr, 1984). The positive and negative charges build an electric field on the PAN/TiO_2 nanofiber (Jiang et al., 2021). In the effect of electric field, the photo-generated electrons and holes of TiO_2 can migrate to the surface of TiO_2 in order. The photo-generated electrons can be can effectively distributed in two different areas with effect of electric field shown in the Fig. 8. It would prevent the combination of photo-generated carriers. With much more efficiency of photogenerated carries, the carries in the TiO_2 can react with target reactant on its surface and produce much more O_2- and •OH radicals and get a better photocatalytic activity (Li et al., 2015a; Li et al., 2015b; Zalfani et al., 2017). Our experimental results and these reasonable considerations explain the enhanced photocatalytic activity of PAN/TiO_2 composite nanofiber mats for degradation of RhB under the vibration-light.

4. Conclusion

In conclusion, the PAN/TiO_2 nanofiber mat with the different contents of TiO_2 or PAN were synthesized by the electrospinning. The photocatalytic activities of degradation of RhB could be significantly improved with the piezoelectricity of PAN/TiO_2 nanofiber mat caused by environmental mechanical vibration. The effect of vibration energy on the photocatalytic activity increased with the increasing PAN contents in the PAN/2TiO_2. With 8 wt% of TiO_2 in the PAN/TiO_2 nanofibers, it exhibited best performance on improving the photocatalytic activity by the piezoelectricity. The mechanism for enhanced photocatalytic activity by the vibration can be attributed to the effect of piezoelectricity of PAN polymer on the TiO_2. The present results and design of catalysts provide new insights for enhancing photocatalytic activity of catalysis mat by the effect of piezoelectric properties of polymers.

CRediT authorship contribution statement

Deng Ding: Conceptualization, Methodology, Data curation, Writing-Original draft preparation. *Zhiwei Li*: Investigation, Analysis of Data, Original draft Editing. *Sooyung Yu*: Soft of Material Characterization. *Bingxin Yang*: Validation, Language Modification. *Yadong Yin*: Supervision, Methodology. *Ling Zan*: Supervision, Methodology, Financial Support. Nosang Vincent Myung*: Supervision, Methodology, Financial Support, Writing-Reviewing and Editing.

Declaration of competing interest

The authors declare that they have no known competing financial interests or personal relationships that could have appeared to influence the work reported in this paper.

Acknowledgment

This work was jointly supported by the National Science Foundation (NSF CBET #2040464), The Natural Science Foundation of Province, China (No. 2021CFB218) and the Key Research and Development Project of Hubei Province. (No. 2020BBB068). Deng thanks the financial support from the National Natural Science Foundation of China (52102111).

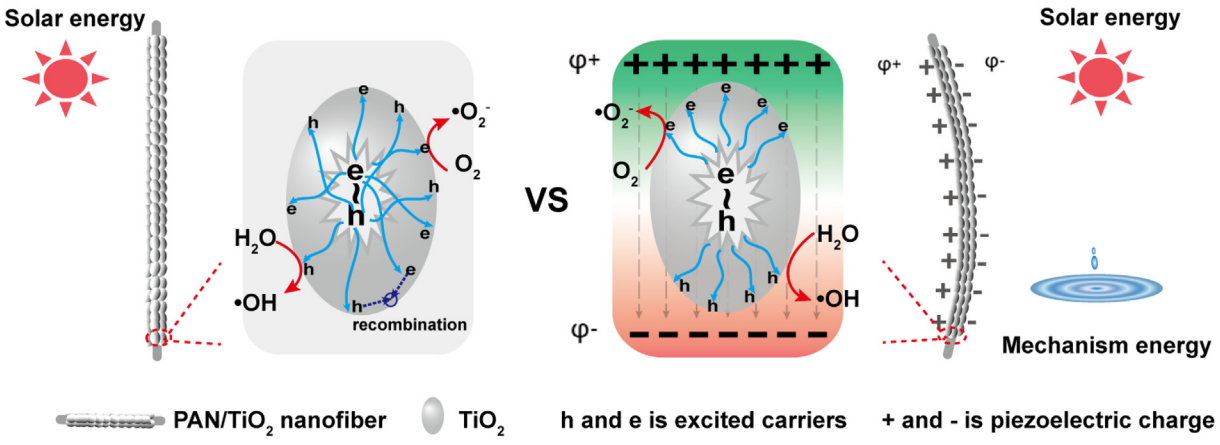

Fig. 8. The mechanism of effect of piezo of PAN on the photocatalyst of TiO_2.

Appendix A. Supplementary data

Supplementary data to this article can be found online at https://doi.org/10.1016/j.scitotenv.2022.153790.

References

<1-s2.0-S138589472102739X-main.pdf>.

Amiri, O., Salar, K., Othman, P., Rasul, T., Faiq, D., Saadat, M., 2020. Purification of wastewater by the piezo-catalyst effect of PbTiO3 nanostructures under ultrasonic vibration. J. Hazard. Mater. 394, 122514.

Brillas, E., Martínez-Huitle, C.A., 2015. Decontamination of wastewaters containing synthetic organic dyes by electrochemical methods.An updated review. Appl. Catal. B: Environ. 166, 603–643.

Chen, X., Liu, L., Feng, Y., Wang, L., Bian, Z., Li, H., Wang, Z.L., 2017. Fluid eddy induced piezo-promoted photodegradation of organic dye pollutants in wastewater on ZnO nanorod arrays/3D Ni foam. Mater. Today 20, 501–506.

Chen, F., Huang, H., Guo, L., Zhang, Y., Ma, T., 2019. The role of polarization in photocatalysis. Angew. Chem. Int. Ed. 58, 10061–10073.

Chen, J., Lei, H., Ji, S., Wu, M., Zhou, B., Dong, X., 2021. Synergistic catalysis of BiOIO3 catalyst for elimination of organic pollutants under simultaneous photo-irradiation and ultrasound-vibration treatment. J. Colloid Interface Sci. 601, 704–713.

Chorsi, M.T., Curry, E.J., Chorsi, H.T., Das, R., Baroody, J., Purohit, P.K., Ilies, H., Nguyen, T.D., 2019. Piezoelectric biomaterials for sensors and actuators. Adv. Mater. 31, 1802084.

Chou, Y., Shao, C., Li, X., Su, C., Xu, H., Zhang, M., Zhang, P., Zhang, X., Liu, Y., 2013. BiOCl nanosheets immobilized on electrospun polyacrylonitrile nanofibers with high photocatalytic activity and reusable property. Appl. Surf. Sci. 285, 509–516.

Crossland, E.J., Noel, N., Sivaram, V., Leijtens, T., Alexander-Webber, J.A., Snaith, H.J., 2013. Mesoporous TiO_2 single crystals delivering enhanced mobility and optoelectronic device performance. Nature 495, 215–219.

Ding, D., Jiang, Z., Ji, D., Myung, N.V., Zan, L., 2020. Bi_2O_2Se as a novel co-catalyst for photocatalytic hydrogen evolution reaction. Chem. Eng. J. 400, 125931.

Gao, W., Ran, C., Wang, M., Li, L., Sun, Z., Yao, X., 2016. The role of reduction extent of graphene oxide in the photocatalytic performance of Ag/AgX (X= Cl, Br)/rGO composites and the pseudo-second-order kinetics reaction nature of the Ag/AgBr system. Phys. Chem. Chem. Phys. 18, 18219–18226.

Greenstein, K.E., Myung, N.V., Parkin, G.F., Cwiertny, D.M., 2019. Performance comparison of hematite (alpha-Fe_2O_3)-polymer composite and core-shell nanofibers as point-of-use filtration platforms for metal sequestration. Water Res. 148, 492–503.

Hisatomi, T., Kubota, J., Domen, K., 2014. Recent advances in semiconductors for photocatalytic and photoelectrochemical water splitting. Chem. Soc. Rev. 43, 7520–7535.

Huang, M., Xu, C., Wu, Z., Huang, Y., Lin, J., Wu, J., 2008. Photocatalytic discolorization of methyl orange solution by Pt modified TiO_2 loaded on natural zeolite. Dyes Pigments 77, 327–334.

Ico, G., Myung, A., Kim, B., Myung, N., Nam, J., 2018. Transformative piezoelectric enhancement of P (VDF-TrFE) synergistically driven by nanoscale dimensional reduction and thermal treatment. Nanoscale 10, 2894–2901.

Jiang, Y., Li, M., Mi, Y., Guo, L., Fang, W., Zeng, X., Zhou, T., Liu, Y., 2021. The influence of piezoelectric effect on the heterogeneous photocatalytic hydrogen production of strontium titanate nanoparticles. Nano Energy 85, 105949.

Lan, S., Zeng, X., Rather, R.A., Lo, I.M.C., 2019. Enhanced trimethoxypyrimidine degradation by piezophotocatalysis of BaTiO3/Ag3PO4 using mechanical vibration and visible light simultaneously. Environ. Sci. Nano 6, 554–564.

Li, H., Zhou, Y., Tu, W., Ye, J., Zou, Z., 2015. State-of-the-art progress in diverse heterostructured photocatalysts toward promoting photocatalytic performance. Adv. Funct. Mater. 25, 998–1013.

Li, Q., Li, X., Wageh, S., Al-Ghamdi, A.A., Yu, J., 2015. CdS/graphene nanocomposite photocatalysts. Adv. Energy Mater. 5, 1500010.

Liang, Z., Yan, C.-F., Rtimi, S., Bandara, J., 2019. Piezoelectric materials for catalytic/photocatalytic removal of pollutants: recent advances and outlook. Appl. Catal. B Environ. 241, 256–269.

Lin, P., Chen, X., Yan, X., Zhang, Z., Yuan, H., Li, P., Zhao, Y., Zhang, Y., 2014. Enhanced photoresponse of Cu_2O/ZnO heterojunction with piezo-modulated interface engineering. Nano Res. 7, 860–868.

Ma, J., Ren, J., Jia, Y., Wu, Z., Chen, L., Haugen, N.O., Huang, H., Liu, Y., 2019. High efficiency bi-harvesting light/vibration energy using piezoelectric zinc oxide nanorods for dye decomposition. Nano Energy 62, 376–383.

Mushtaq, F., Chen, X., Hoop, M., Torlakcik, H., Pellicer, E., Sort, J., Gattinoni, C., Nelson, B.J., Pané, S., 2018. Piezoelectrically enhanced photocatalysis with $BiFeO_3$ nanostructures for efficient water remediation. Iscience 4, 236–246.

Nalbandian, M.J., Cwiertny, D.M., Myung, N.V., 2012. Synthesis and optimization of photocatalytic TiO_2 nanofibers for treatment of impaired water supplies. Abstr. Pap. Am. Chem. Soc. 244.

Nalbandian, M.J., Zhang, M.L., Sanchez, J., Kim, S., Choa, Y.H., Cwiertny, D.M., Myung, N.V., 2015. Synthesis and optimization of Ag-TiO_2 composite nanofibers for photocatalytic treatment of impaired water sources. J. Hazard. Mater. 299, 141–148.

Nalbandian, M.J., Greenstein, K.E., Shuai, D.M., Zhang, M.L., Choa, Y.H., Parkin, G.F., Myung, N.V., Cwiertny, D.M., 2015. Tailored synthesis of photoactive TiO_2 nanofibers and Au/TiO_2 nanofiber composites: structure and reactivity optimization for water treatment applications. Environ.Sci.Technol. 49, 1654–1663.

Nonnenmann, S.S., Leaffer, O.D., Gallo, E.M., Coster, M.T., Spanier, J.E., 2010. Finite curvature-mediated ferroelectricity. Nano Lett. 10, 542–546.

Ong, W., Tan, L.L., Ng, Y.H., Yong, S.T., Chai, S.-P., 2016. Graphitic carbon nitride (g-C_3N_4)-based photocatalyst for artificial photosynthesis and environmental remediation: are we a step closer to achieving sustainability. Chem. Rev. 116, 7159–7329.

Ou, G., Li, Z., Li, D., Cheng, L., Liu, Z., Wu, H., 2016. Photothermal therapy by using titanium oxide nanoparticles. Nano Res. 9, 1236–1243.

Peter, K.T., Vargo, J.D., Rupasinghe, T.P., De Jesus, A., Tivanski, A.V., Sander, E.A., Myung, N.V., Cwiertny, D.M., 2016. Synthesis,optimization, and performance demonstration of electrospun carbon nanofiber-carbon nanotube composite sorbents for point-of-use water treatment. ACS Appl. Mater. Interfaces 8, 11431–11440.

Raziq, F., Sun, L., Wang, Y., Zhang, X., Humayun, M., Ali, S., Bai, L., Qu, Y., Yu, H., Jing, L., 2018. Synthesis of large surface-area g-C_3N_4 comodified with MnOx and Au-TiO_2 as efficient visible-light photocatalysts for fuel production. Adv. Energy Mater. 8, 1701580.

Senthamizhan, A., Balusamy, B., Aytac, Z., Uyar, T., 2016. Grain boundary engineering in electrospun ZnO nanostructures as promising photocatalysts. CrystEngComm 18, 6341–6351.

Shi, M., Li, G., Li, J., Jin, X., Tao, X., Zeng, B., Pidko, E.A., Li, R., Li, C., 2020. Intrinsic facet-dependent reactivity of well-defined BiOBr nanosheets on photocatalytic water splitting. Angew. Chem. Int. Ed. 59, 6590–6595.

Shuai, D.M., Nalbandian, M., Choa, Y.H., Myung, N.V., Cwiertny, D.M., 2013. Optimizing photocatalytic performance of electrospun TiO_2 nanofibers for removal of emerging organic contaminants. Abstr. Pap. Am. Chem. Soc. 245.

Tu, S., Guo, Y., Zhang, Y., Hu, C., Zhang, T., Ma, T., Huang, H., 2020. Piezocatalysis and piezophotocatalysis: catalysts classification and modification strategy,reaction mechanism, and practical application. Adv. Funct. Mater. 30, 2005158.

Ueda, H., Carr, S., 1984. Piezoelectricity in polyacrylonitrile. Polym. J. 16, 661–667.

Wang, K., Shao, C., Li, X., Miao, F., Lu, N., Liu, Y., 2016. Heterojunctions of p-BiOI nanosheets/n-TiO_2 nanofibers: preparation and enhanced visible-light photocatalytic activity. Materials 9, 90.

Wang, D., Li, Z., Zhou, J., Fang, H., He, X., Jena, P., Zeng, J.-B., Wang, W.-N., 2018. Simultaneous detection and removal of formaldehyde at room temperature: Janus Au@ZnO@ZIF-8 nanoparticles. Nano-micro Lett. 10, 4.

Wang, W., Zheng, Y., Jin, X., Sun, Y., Lu, B., Wang, H., Fang, J., Shao, H., Lin, T., 2019. Unexpectedly high piezoelectricity of electrospun polyacrylonitrile nanofiber membranes. Nano Energy 56, 588–594.

Xi, X., Wang, J., Dong, X., Ma, Q., Yu, W., Liu, G., 2014. Flexible Janus nanofiber: a new tactics to realize tunable and enhanced magnetic-luminescent bifunction. Chem. Eng. J. 254, 259–267.

You-ji, L., Wei, C., 2011. Photocatalytic degradation of Rhodamine B using nanocrystalline TiO_2–zeolite surface composite catalysts: effects of photocatalytic condition on degradation efficiency. Catal. Sci. Technol. 1, 802.

Yu, S., Myung, N.V., 2018. Minimizing the diameter of electrospun polyacrylonitrile (PAN) nanofibers by design of experiments for electrochemical application. Electroanalysis 30, 2330–2338.

Yu, L., Shao, Y., Li, D., 2017. Direct combination of hydrogen evolution from water and methane conversion in a photocatalytic system over Pt/TiO_2. Appl. Catal. B Environ. 204, 216–223.

Zalfani, M., Hu, Z.-Y., Yu, W.-B., Mahdouani, M., Bourguiga, R., Wu, M., Li, Y., Van Tendeloo, G., Djaoued, Y., Su, B.-L., 2017. $BiVO_4$/3DOM TiO_2 nanocomposites: effect of $BiVO_4$ as highly efficient visible light sensitizer for highly improved visible light photocatalytic activity in the degradation of dye pollutants. Appl. Catal. B Environ. 205, 121–132.

Zeng, X., Bai, Y., Choi, S., Tong, L., Aleisa, R., Li, Z., Liu, X., Yu, R., Myung, N., Yin, Y., 2019. Mesoporous TiO_2 nanospheres loaded with highly dispersed Pd nanoparticles for pH-universal hydrogen evolution reaction. Mater. Today Nano 6, 100038.

Zhao, Y., Huang, X., Gao, F., Zhang, L., Tian, Q., Fang, Z.-B., Liu, P., 2019. Study on water splitting characteristics of CdS nanosheets driven by the coupling effect between photocatalysis and piezoelectricity. Nanoscale 11, 9085–9090.

Zhou, D., Chen, Z., Yang, Q., Dong, X., Zhang, J., Qin, L., 2016. In-situ construction of all-solid-state Z-scheme g-C3N_4/TiO_2 nanotube arrays photocatalyst with enhanced visible-light-induced properties. Sol. Energy Mater. Sol. Cells 157, 399–405.

Zhou, X., Shao, C., Yang, S., Li, X., Guo, X., Wang, X., Li, X., Liu, Y., 2018. Heterojunction of g-C_3N_4/BiOI immobilized on flexible electrospun polyacrylonitrile nanofibers: facile preparation and enhanced visible photocatalytic activity for floating photocatalysis. ACS Sustain. Chem. Eng. 6, 2316–2323.